Chapter 8

Early Corrosion Fatigue Damage on Stainless Steels Exposed to Tropical Seawater: A Contribution from Sensitive Electrochemical Techniques

Narciso Acuña-González, Jorge A. González-Sánchez, Luis R. Dzib-Pérez and Aarón Rivas-Menchi

Additional information is available at the end of the chapter

http://dx.doi.org/10.5772/52698

1. Introduction

A major concern in the design of engineering structures is the ability of components to maintain their integrity during their entire life service even when subjected to a combination of fluctuating loads and aggressive environments. The requirement for reliable structural integrity is particularly important for structures, involved in fundamental fields such as transportation, oil and gas production and energy generation. Fatigue and corrosion fatigue failures take place in components and structures as result of complex loading histories. There are different stages of fatigue damage in engineering components where defects may nucleate on initially smooth or undamaged sections, followed by microstructural crack formation, stable propagation and finally unstable crack propagation where catastrophic failure occurs.

Total fatigue life is often considered as a process of fourth major stages [1,2]:

a. Initiation or nucleation of fatigue cracks: substructural and microstructural which cause nucleation or permanent damage,
b. Small-Crack growth: the creation and growth of microscopic cracks,
c. Macro-Crack propagation: the growth and coalescence of microscopic flaws to form "dominant cracks" and stable propagation of dominant macrocracks
d. Final fracture: structural instability or complete fracture.

Then, fatigue life of engineering components and structures can be defined as the period during which cracks initiate from defects and propagate. The largest fraction of fatigue life

is spent in the crack propagation stage. However, when engineering structures operate under severe conditions, the problem of fatigue failure is raised, especially in presence of aggressive environments. Under such severe conditions, the crack initiation stage is dramatically reduced as the case of structures in marine environments.

On the other hand, the stresses operating on structures can be mechanically applied (constant or cyclic), residual, and in some cases, thermal which depend on the operation conditions.

Stainless steels are an important group of materials for diverse engineering applications. This kind of corrosion resistant materials was introduced with the aim of reducing maintenance costs involved with materials such as carbon steel. However, there are several cases around the world, [3-8] in which the failure frequency of stainless steel piping systems on offshore platforms is very high, resulting in unacceptable maintenance costs.

Unfortunately the degradation process is more complex than just localized electrochemical reactions at the metal surface. It is documented [5,9,10] that the corrosion of stainless steels (SS) is more severe in natural seawater than in sterile or synthetic seawater due to microorganisms activity. There is agreement among researchers that the increased corrosion is due to biofilm formation [4,5,7,8]. Electrochemical reactions are influenced by the chemical micro-environments generated by formation of biofilms at the metal surface. In seawater applications, the most widely used stainless steel grade, namely, 316L, suffers from localized corrosion. Even the substantial amount of data published about studies of localized corrosion of 316 and 316L stainless steels, frequently affected by pitting and crevice corrosion, the problem of structural failure in marine environments remains.

An outstanding problem in corrosion science and engineering involves the prediction, of damage caused by corrosion fatigue during the early stages of damage. This problem is particularly important because localized attack, such as pitting corrosion fatigue (PCF), normally occurs on passive alloys with minimal metal weight loss, and is commonly detected when the failure of the component is complete.

The most important aspect of corrosion fatigue assessment on components and structures in real service is the prediction of their residual life when there is a risk of undergoing localized attack as precursor of fatigue cracks. The conventional fracture mechanics tools are limited to provide information concerning the type and rate of damage occurring during the early stages of damage and consequently provide limited insight into the mechanism of pitting corrosion fatigue failure process. It is important to understand the role of the environment on the early stages of corrosion fatigue damage. In this sense, very sensitive electrochemical techniques have been used in corrosion fatigue studies by the authors of this chapter, where the main aim has been to determine the early stages of corrosion fatigue damage. This chapter presents a review of information obtained from applied sensitive electrochemical techniques to stainless steels exposed to seawater and chloride ions media to observe Early Corrosion Fatigue Damage.

2. Corrosion fatigue

The *S-N* approach to fatigue studies is usually appropriate for situations where a component or structure can be considered a continuum (i.e., cracks-free assumption). However, the fatigue process leading to failure is generally represented in terms of crack initiation stage followed by crack propagation to critical size.

It must be recognized, however, that there is no generally accepted definition as to what constitutes initiation or when the initiation phase is complete and propagation commences. The net cycles to failure represents the sum of both, crack initiation and propagation.

$$Total\ fatigue\ life = Ni + Np \quad (1)$$

where ***N*i** represents the number of cycles for crack initiation and ***N*p** the number of cycles for crack propagation to failure**.** A major difficulty with regard to fatigue research involves the large number of variables which influence the phenomenon. These may be divided into three general variables categories [11,12]:

a. Mechanical
b. Material
c. Environmental

The complex task associated with fatigue resistance evaluation is the fact that individual factors may be synergically interactive, so a change in one must be assumed to affect the role of the others. Thus, the accumulation of damage during the fatigue lifetime of a component depends not only on its load history, but also of the synergistic effects of stress and surrounding environment [13,14]. Then, corrosion fatigue is defined as a synergistic effect in which corrosion and fatigue occur simultaneously. The combined effect of an aggressive environment, such as seawater, with a cyclic stress or strain is, invariably, more severe than the sum of the two effects of corrosion and fatigue acting separately. The effect of the environment on fatigue resistance is well documented in the form of stress vs number of cycles to failure (*S-N*) curves which show that, for the majority of the cases, the environment removes the fatigue limit (Figure 1). It has been shown that many corrosion fatigue failures of stainless steels in seawater are induced in the early stages of damage by pitting corrosion [15-18].

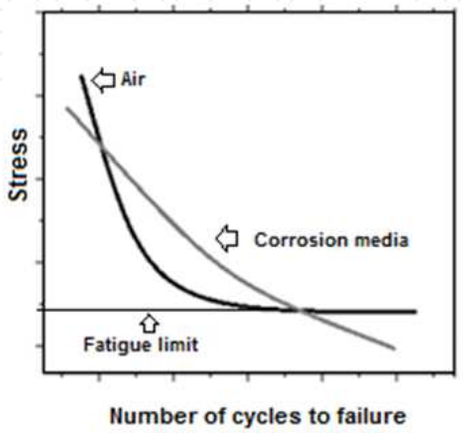

Figure 1. Schematic of *S-N* curve presenting air fatigue and corrosion fatigue behavior.

Fatigue and CF studies address the following regimes:

a. LEFM (long crack) regime, were cracks are of the order of millimeters (i.e. propagation)
b. EPFM (physical short cracks) regime, were cracks of the order hundreds of micrometers
c. MFM (short crack) regime, were cracks of the order of tends of micrometers develop early in the lifetime and exhibit growth rate variations through the microstructure (i.e. nucleation).

The most important aspect of corrosion fatigue assessment on components and structures in real service is the prediction of their residual life when there is a risk of undergoing localized attack as precursor of fatigue cracks.

In passive alloys, it is recognized that pitting corrosion plays a very important role in CF crack initiation [16, 17, 19]. CF lifetime prediction turns complex because of the need to account main processes leading to fatigue failure from a 'defect-free' surface [14, 20], where the early corrosion fatigue damage includes:

i. breakdown of the surface passive film
ii. pit initiation and growth,
iii. transition from pit to short crack nucleation,
iv. short crack growth

The selection of the techniques used to evaluate and study corrosion depends on the kind of corrosion taking place. The principal aim of the corrosion scientist is to determine the mechanism of the corrosion process including intermediate reactions and the kinetics of these processes. Sometimes it is necessary to use intrusive methods (electrochemical methods) in which the system is stimulated externally and the response of the system to that perturbation is measured. Other techniques are able to measure electrochemical activity without the necessity of any kind of external perturbation to the system, the electrochemical noise technique (ENT), the scanning reference electrode technique (SRET) and scanning vibrating electrode technique (SVET) are examples of non-intrusive techniques. The most important aspect of corrosion assessment on components and structures in real service is the prediction of their residual life when there is a risk of undergoing localized attack. In that respect the use of electrochemical methods for studying localized corrosion is an important part of the evaluation since the kinetics of localized corrosion is different with respect to general (uniform) corrosion.

From a structural integrity point of view general corrosion does not represent a serious problem for the corrosion engineer due to the fact that stress concentrators are not generated. Therefore general corrosion can be assessed using basic electrochemistry concepts and techniques [21,22]. In the case of localized corrosion, the measurement of the corrosion rate becomes more complicated due to unequal anodic and cathodic area ratios and therefore the effects of this kind of damage on the structural integrity of structures are much more severe.

2.1. Localized corrosion concepts

Due to their recurrent nature, localized corrosion processes often cause major practical problems affecting the performance of technologically important metallic materials, like stainless steels, nickel, aluminium, and many others metals and their alloys in different environments, especially those containing chlorides.

It can be considered that the corrosion process results from changes in the nature and composition of metals exposed to environments of homogeneous composition. The point of interest is "what happens when metals with approximately uniform composition are exposed to electrolytic environments in which composition changes makes them heterogeneous, e.g. differential aeration?" In this case we are dealing with concentration cells, i.e. localised corrosion.

One of the established essential principles of corrosion is that: The sum of the rates of the cathodic reactions must be equal to the sum of the rates of the anodic reactions, irrespective of whether the attack is uniform or localized [21], so the following equation must be satisfied:

$$\sum I_a = \sum I_c \tag{2}$$

where I_c and I_a denote the cathodic and anodic currents respectively which has a direct relation with the reaction rate of the electrochemical process.

If it is considered that the attack is uniform and assuming that there is only a single predominant anodic and cathodic reaction, then:

$$I_a / S_a = I_c / S_c \text{ or } i_a = i_c \tag{3}$$

where i_a and i_c are the anodic and cathodic current densities assuming the area of the cathode S_c equals the area of the anode S_a.

When the corrosion attack is localized the anode area is very small compared with the cathode area, $S_a < S_c$ and as a consequence $i_a > i_c$, and the larger the ratio i_a:i_c, the more intensive the attack. Thus localized attack usually involves a corrosion cell consisting of a large cathodic area and a small anodic area.

It is now known that many aqueous corrosion processes of great technical interest occur under conditions in which the access of electrolyte is restricted. This can be due to the special geometry of the corroding material e.g. structures with riveted plates, flange joints, gaskets; and also due to the existence of some deposits such as corrosion products or scales on the corroding surface. In the cases where corrosion occurs under conditions of restricted diffusion, the chemical composition of the corroding environment inside the occluded cavity may be very different from that of the composition of the bulk solution. One of the most important effects is that changes in oxygen or ionic concentration in the electrolyte give rise to changes in corrosion potential. Under normal circumstances where the aggressive environment is aerated, the surface of the corroding alloy outside the occluded cavities is

often passive as a result of the formation of an oxide film of corrosion products. Passivation takes place at these sites because they are in direct contact with the oxygen dissolved within the electrolyte. These surfaces act as aerated cathodes where oxygen takes part in the reduction reaction of the corrosion process. In this reaction the oxygen is reduced with the consequent increase of pH according to the following reaction for the case of basic or neutral solutions [23]:

$$O_2 + 2H_2O + 4e^- \rightarrow 4OH^- \tag{4}$$

or in a solution of low pH:

$$O_2 + 4H^+ + 4e^- \rightarrow 2H_2O \tag{5}$$

The surface, which is inside the occluded cavity, is active and acts as anode as a consequence of the very low concentration of oxygen in the solution inside the cavity. At these surfaces the metal undergoes dissolution. Additionally, the hydrolysis reaction takes place with a decrease in the pH of the solution according to the following reaction sequence:

for iron,

$$Fe \rightarrow Fe^{++} + 2e^- and\ 3Fe^{++} + 4H_2O \rightarrow Fe_3O_4 + 8H^+ + 2e^- \tag{6}$$

Much effort has been made in the last 40 years for a better understanding of the processes involved in localized corrosion, the majority of these studies being focused principally on aspects of the growth and stability of the sites undergoing localized attack. On the other hand, the mechanisms of nucleation and early stages of damage are not yet completely understood.

An important improvement on the present state of knowledge is achieved when the global process of localized corrosion can be partitioned into a nucleation stage (initiation), and a successive metastable growth stage, which eventually is followed either by rapid repassivation or stable pit growth. If the active condition inside a crevice or pit is stable over a longer period of time, rapid metal dissolution usually takes place. The rate controlling reaction during the localized corrosion processes such as activation, diffusion, or ohmic control, has a significant influence on the shape and geometry of the crevices or pits produced.

The theoretical models, that have been proposed to describe the initiation of the localized corrosion process, can be grouped into [24,25]:

- Adsorption mechanisms
- Ion migration and penetration models
- Mechanical film breakdown theories.

Substantial research has been carried out to study the structural parameters involved in localized corrosion processes. From these, it has been demonstrated that defects in the metal structure, such as non-metallic inclusions or dislocations may generally act as sites for pit

initiation on passive metal surfaces [26]. Stainless Steels (SS's) with higher concentrations of alloying elements were found to have an increased pitting resistance due to the formation of passive films containing fewer defects and greater stability.

Despite the efforts made to understand this phenomenon, localized corrosion is a non-predictable degradation process of metals and alloys in contact with aggressive environments. Given that most of the information related to the stable stage of localized corrosion has been obtained throughout studies of pitting and crevice corrosion, this aspect of the localized attack will be presented in the next section dedicated to pitting corrosion.

3. Pitting corrosion fatigue

3.1. Breakdown of the surface passive film

Corrosion is an electrochemical reaction process between a metal or metal alloy and its environment [27], which involves complex mass and charge transfer taking place at the metal-electrolyte interface. These charge transfer reactions at the interface are the origin of the instability of metals. The high corrosion resistance of Austenitic SS's is primarily attributed to the adherent metal-oxide film formed on its surface called passive film. This natural coating acts as a barrier that avoids the contact between fresh metal surface and the electrolyte limiting the corrosion reaction and such alloy is said to be passive. When stainless steels are exposed to oxygen containing electrolytes, a chemically stable, non soluble film is formed from a mixture of iron and chromium oxides, with hydroxide and water-containing compounds located in the outermost region of the film, and chromium oxide enrichment at the metal-film interface [28]. However, the resistance of this passive film is determined by the environmental conditions to which the SS is exposed to, as well as by the alloy composition. Many metals and alloys become covered with oxide films on exposure to aqueous environments. Copper, aluminum or tin and their alloys develop thick films, while metals which exhibit passive behaviour like stainless steels have a very thin film of the order of 9 to 20 nm. The passive films are cathodic to the metal matrix. However, the susceptibility of passive films to suffer local breakdown depends upon the nature of the film, the quantity and nature of non metallic inclusions, the chemical composition of the electrolyte or solution, and the electrochemical state at the metal/solution interface, but also to a possible stress state.

For CF test, when the passive metal or alloy is subjected to cyclic loading, the passive film is damaged mechanically due to the creation of slip steps from beneath and following a repeated process of microdeformation-activation-dissolution-repassivation.

During the initial cyclic loading, fine slip lines appear on the specimen surface because dislocations, at or near the surface, the stress in localized sites can exceed the nominal stress. By using microscopic techniques has been possible to observe localized plasticity at microscopic scale in the grains, where fatigue damage is caused by microplasticity produced by large shear stresses.

Processes of nucleation and formation of fatigue slips bands often precedes at grain boundaries as is shown in figure 2. Mughrabi et al. [29] showed that nucleation at grain boundaries occur at sites where persistent slip bands (PSBs) impinge.

In smooth surfaces of SS's, during the early corrosion fatigue damage, the permanent slip bands are associated with breakdown of the passive film. The breakdown of the passive film causes dissolution of the non-covered active metal in contact with the electrolyte, which acts as a small anode against the large cathodic. This small anode is a vulnerable area on the metal surface, where a high local metal dissolution takes place, and leading cavities such as pits and/or crevice. Extensive development of techniques to study electrochemical reactions have simulated the analysis of potential and current fluctuations taking place during electrochemical processes which are translated in to electrochemical noise (EN) signals.

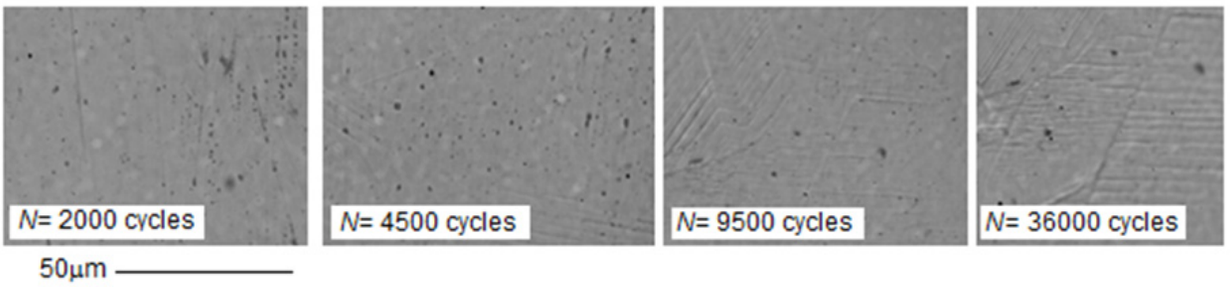

Figure 2. Evolution of fatigue slip bands in a 316L SS during cycling stress in air, under σ_{max}=217 MPa (90%$\sigma_{0.2}$), load frequency ω=1.0 Hz and a stress ratio R=0 conditions.

EN is defined as spontaneous fluctuations in current and potential generated by corrosion reactions [30-34]. In this context, the study of spontaneous current or potential fluctuations to characterize corrosion processes have received considerable attention, such as the study of corrosion potential (E_{corr}) and current fluctuations applied to monitor the onset of events characterizing pitting [35-36] or stress corrosion cracking (SCC) [37-39] The noise is typically measured potentiostatically, galvanostatically, or in a Zero Resistance Ammeter (ZRA) mode [30,31,34]. With ZRA mode, both the potential and current fluctuations can be measured using two nominally identical electrodes, connected through a ZRA; where a net current and changes in the potential are observed at free corrosion conditions according to the corrosion process.

During the Corrosion Fatigue tests conducted in natural seawater [16], the potential time series obtained from electrochemical noise measurements had a common characteristic pattern of quick drop and slow recovery. Common explanations for these patterns of quick drop and slow recovery have been associated to anodic dissolution, passive film breakdown, metastable and stable pitting corrosion, or with the crack initiation and crack growth due to microstrain and local mechanical stress conditions [16].

The figure 3 shows patterns of quick drop and slow recovery, indicating that passive film eventually is broken, due to applied mechanical stress and the interaction with the electrolyte, turning it in an active dissolution of metal. Also, on figure 3, the surface damage after N=43200 cycles of corrosion fatigue tests can be observed. In 316L SS-natural seawater

system, current transients for unstressed conditions reaches average values in current density around 0.20 μA.cm^{-2}, while under cyclic stress conditions it ranges between 0.25 to 0.85 μA.cm^{-2} [16].

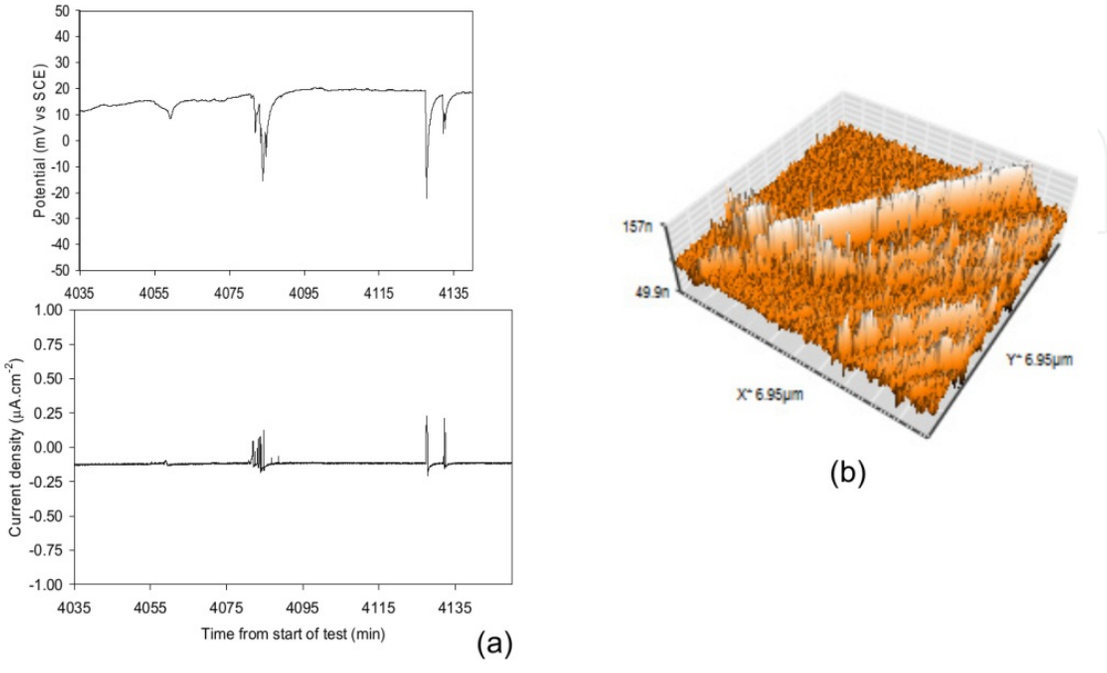

Figure 3. a) Potential and current noise profiles [16] and b) AFM surface image, for a 316L SS exposed to natural seawater under an induced cyclic stress of $\Delta\sigma$ = 140 MPa (58%$\sigma_{0.2}$), after N=43200 cycles, at a load frequency ω=0.17 Hz and stress ratio R=0.

3.2. Pit nucleation and growth

Pit nucleation

According to Szklarska-Smialowska [34], the susceptibility of a metal or alloy to pitting can be estimated by determination of one of the following criteria:

- Characteristic pitting potential
- Critical pitting temperature,
- Number of pits per unit area, or weight loss and
- The lowest concentration of chloride ions that may cause pitting

One of the most important parameter to determine an alloy's susceptibility to pitting corrosion is the pitting potential, i. e., the potential at which the passive film starts to break down locally. The potential above which pits nucleate is denoted by E_p and the potential below which pitting does not occur and above which the nucleated pits can grow is often indicated by E_{pp} (Figure 4 and Table 1).

As mentioned above, pitting corrosion involves localised attack of very small areas of metal surface undergo localised attack whilst the rest of the surface is largely unaffected and remains passive. Pitting is a particularly insidious form of localized corrosion because

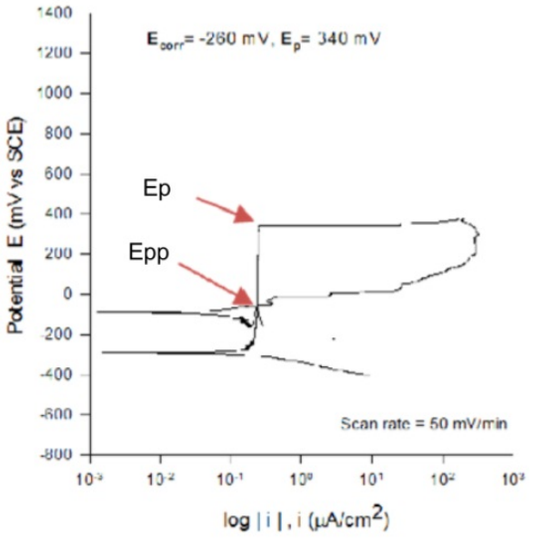

Figure 4. Arrows indicate the E_P and E_{pp} on the polarization curve [40].

SS Alloy	(E_{corr})* (mV vs SCE)	(E_P)* (mV vs SCE)	($i_{passive}$)* (μA/cm²)
304 SS	- 260 to – 270	290 to 350	0.3 to 0.4
316L SS	-220 to -260	270 to 320	0.3 to 0.5
Duplex SS	-280 to -310	1060 to 1110	0.3 to 0.5

* Range of values for Ecorr, EP and *i*passive were obtained from five tests under identical experimental conditions.

Table 1. Values of electrochemical parameters for Stainless Steels in artificial seawater, at 26°C and pH 8.2 [40]

the extent of metal dissolution reaction is small but the attack is rapid and penetrates into the metal. The location of pits on metals that develop passive films is often unpredictable, and the pits tend to be randomly dispersed on the metal surface [41-43]. However, Sedriks [44,45] indicates the importance of different types of heterogeneities at the material surface during pit initiation, because the location of pits is to some extent defined by the microstructure of the alloy and the geometry of the system. In chloride containing aqueous solutions, the uniform corrosion rate of stainless steels in the passive state is insignificant, i.e. 0.15 to 15.0 μm per year [46]. However, pitting corrosion of this type of alloys is very common in these environments [45], where the local dissolution rate of metal can be up to 12 mm per year [41].

Pitting corrosion can occur when a local breakdown of the passive film takes place in an aqueous solution on a microscopic scale (nucleation process). This process involves small and sudden increments of anodic current, which are characterized by current spikes, leading to oxidation and dissolution of less than 0.01 μm³ of metal. The nucleation process is unstable and in most cases it will stop by the regeneration of the passive film. Another possibility is that a nucleation event develops into the second stage of initiation, i.e. the metastable pit growth. During this step, a gradual and bigger increase of the anodic current

takes place. This stage stops if repassivation of the micro-pit occurs. A volume of up to several μm^3 of metal can be dissolved in stainless steel during the metastable growth. In some cases the metastable pit growth precedes stable pitting. On the other hand, if repassivation of metastable micro-pit does not occur, the growth of stable pits can take place (figure 5).

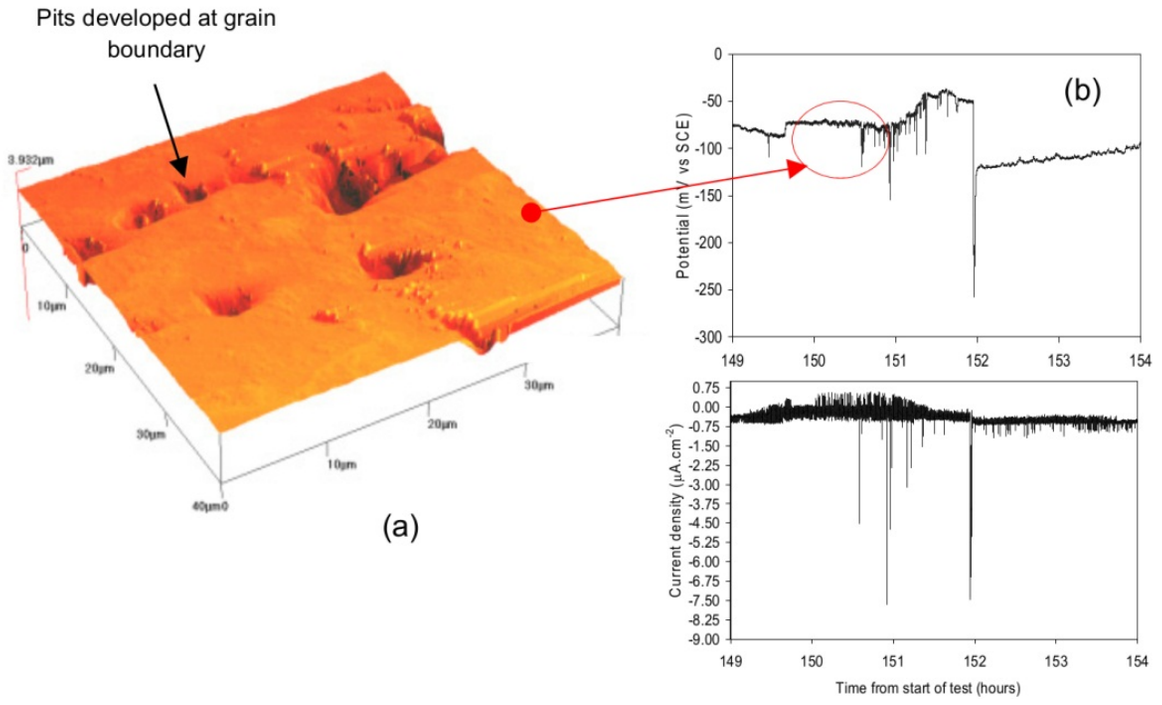

Figure 5. (a) AFM surface image and (b) Potential and current noise profiles for a 316L SS exposed to natural seawater under an induced cyclic stress of $\Delta\sigma$= 140 MPa (58%$\sigma_{0.2}$), after N=86400 cycles, at a load frequency ω=0.17 Hz and stress ratio R=0 [16].

Measurements of the physical separation of anodic and cathodic areas, the currents flowing between them as well as the mapping of potentials in electrolytic solutions have been successfully used for the study of the processes of localized corrosion of different systems [47-53]. A schematic drawing of a local corrosion cell is shown in figure 6.

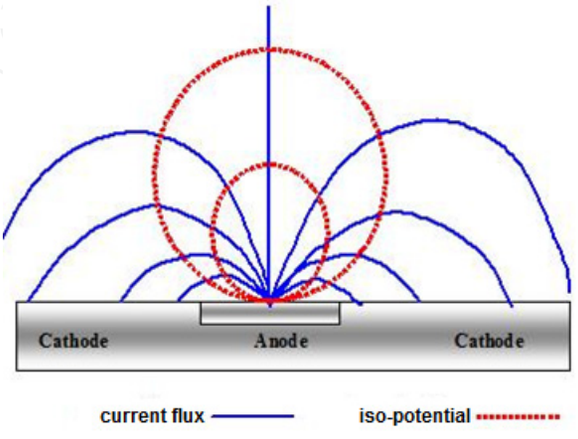

Figure 6. Schematic of current and potential distribution in solution during localized corrosion [40].

With the aim of determining the velocity of metal dissolution directly in active pits during pitting corrosion, Rosenfeld and Danilov [54], designed an apparatus to measure the field strength in the electrolyte directly above an active pit. They employed a twin probe method by using two reference electrodes, which makes it possible to measure the potential difference ΔE in any direction between two points in the electrolyte with the aid of two non-polarizable electrodes, for example calomel electrodes.

The equipment used for the measurements of the potential difference ΔE (ohmic potential gradients) is called the Scanning Reference Electrode (SRET). With the measurement of the electric field strength in the electrolyte over the pits it was possible to determine the current flowing from the anode points, based on the fact that, the vector of the normal component of the current density at a pre-determined point (i') in a uniform field is equal to the product of the electric field strength E and the specific conductivity of the medium κ. The resolution of the SRET depends upon the proximity of the scanning probes to the corroding sites and the magnitude of the corrosion currents from each site. As shall be shown later, the distance between the probe and specimen surface and the conductivity of the solution governs the sensitivity of the technique. It has been reported the capability of the SRET to identify the position of localized activity in the metal surface however did not report any assessment of pit size or shape from the performed SRET measurements [48-51]. The growth of corrosion pits is the next stage of the localized attack process.

Pit growth law

Pit growth studies have received less attention than its initiation. The kinetics of pit growth is generally assessed by electrochemical and metallographic methods. However, a combination of the two methods is usually preferred. A wide variety of pit growth laws have been reported for different systems metal - electrolyte, but the theory of pits growth remains unclear. Although stainless steel 304 is a very common and extensively used alloy, the determination of pit growth in NaCl solutions at open circuit potential has not been possible in terms of reproducible and reliable measurements. This is essentially due to the tendency for spontaneous repassivation of the pits when the steel is at open circuit potential [5]. An approach has been the determination of the pit growth kinetics on potentiostatically generated pits in specific metal – electrolyte systems. Dzib-Pérez [55] generated corrosion pits potentiostatically on specimens type 304 SS in stationary conditions in two electrolytes: 3.5% wtNaCl solution (κ=55.8 mS/cm) and natural seawater (κ=50.6 mS/cm). Specimens were initially polarized potentiostatically in natural seawater for 105 s at a potential of 365 mV vs SCE (to induce the formation of pits) and immediately after, the electrode potential was stepped down to a value of 300 mV vs SCE (to induce the growth of the initially formed pits avoiding the formation of new pits). The chronoamperometries obtained for 304 steel in natural seawater are shown at Figure 7.

All chronoamperometries obtained showed a rapid increase in current during the time the stainless steel specimen was polarized potentiostatically above the pit potential, which is associated to induced nucleation and fast pit growth.

Most of the generated pits quickly repassivated when the potential was stepped down to a potential level below the pitting potential. Under this condition 1 to 3 pits grew steadily

until the end of polarisation. The increase of current as a function of time can be associated with two processes taking place under potentiostatic polarization: mainly the active dissolution of nucleated pits (one to three pits) and the simultaneous dissolution of the metal surface in the passive state. From the integration of the area beneath the curve current vs time the electric charge was obtained, from which the quantity of dissolved metal per pit was calculated using Faraday's law according to the chemical composition of the 304 stainless steel [55].

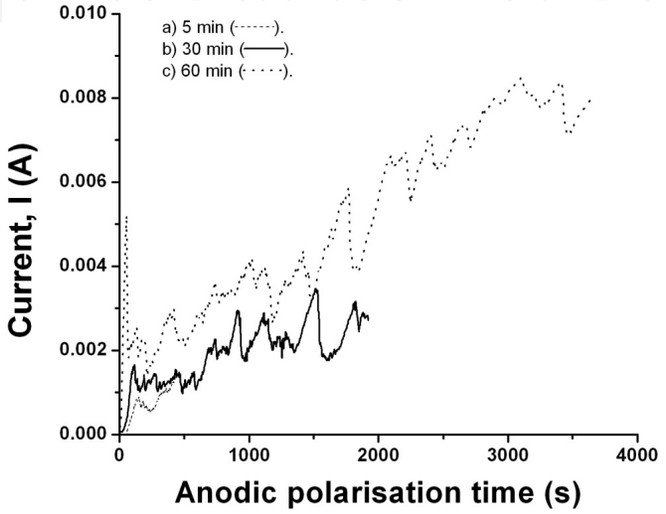

Figure 7. Chronoamperometries obtained during potentiostatic generation of pits in a 304 stainless steel in natural seawater in stationary conditions. Polarisation at 300 mV vs SCE for: a) 5, b) 30 and c) 60 minutes.

And the other hand, Figure 8 shows the amount of material dissolved as function of time of anodic polarization, also includes the fit (solid and dotted lines) performed through the following power equation:

$$DM_{AC} = ct^{d} \tag{7}$$

where DM_{AC} is the amount of dissolved material per pit in μg obtained from chronoamperometries, t is the pit growth time (or anodic polarization time) in minutes and, c and d are constants.

Once determined the amount of dissolved material per pit as a function of anodic polarization time and knowing the density of stainless steel (ρ= 8.03 g/cm^3), the volume of dissolved metal was determined. Using a material removal procedure described in detail by Gonzalez Sanchez and Dzib-Pérez [40-55] to determine the pit depth as a function of time of anodic polarization the empirical pit growth law was established for corrosion pits in 304 stainless steel. Figure 9 shows the Maximum Pit Depth (*MPD*), generated in 304 steel samples, as a function of time under anodic polarisation.

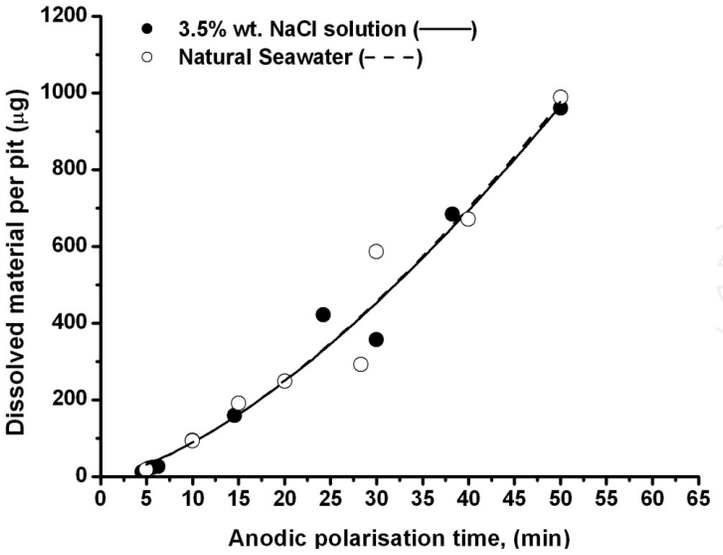

Figure 8. Amount of dissolved material per pit as a function of polarization time for a 304 stainless steel in 3.5% wt NaCl solution (κ=55.8 mS /cm) and in natural seawater (κ=50.6 mS /cm).

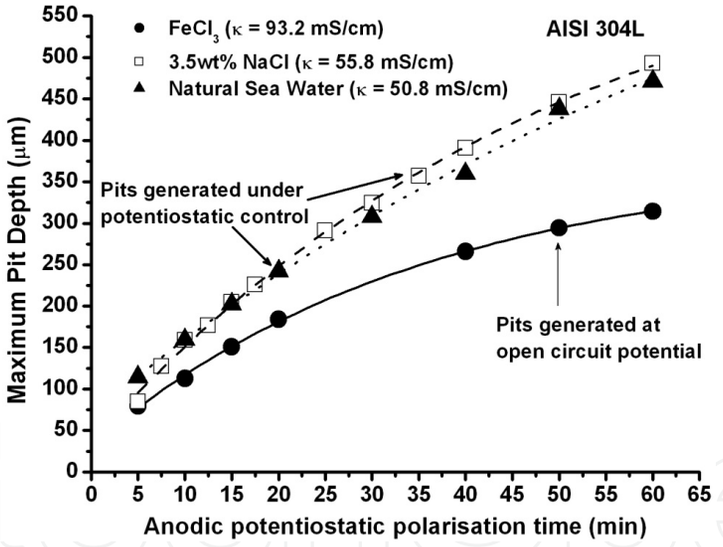

Figure 9. Maximum Pit Depth, as a function of pit growth time, for a 304L stainless steel in electrolytes of different conductivity.

From fitting of these relationships, represented by solid and dotted line, was obtained the empirical equation for the pits growth law for each experimental condition, which has the shape of an exponential equation [55]:

$$P_p = a - bc^t \tag{8}$$

Where *P*p represents the pit depth in μm, and t is the pit growth time in minutes. The values of the constants for the equation 8 are presented in Table 2.

Material	Electrolyte	Conductivity (mS/cm)	Parameter		
			a	b	c
304 SS	Natural seawater	50.6	852.99687	782.72174	0.98796
	3.5% wtNaCl	55.8	692.82813	659.34217	0.98054
	$FeCl_3$	93.2	378.94312	347.10403	0.97224

Table 2. Values of the constants a, b y c from equation 8.

Has been reported that the growth rate of a pit is characterized by a gradual increase in the current at constant potential, which is proportional to t_2 or t_3 [34]. Gonzalez-Sanchez [40] generated pitting on stainless steel 304 and 316L using the same electrochemical process used in this study. This author reported an empirical equation for the pit-growth law of the form $P_d=Kt^{\beta}$ generated under potentiostatic control where P_d is pit depth, t, time and *K* and β are constants depending on the material and the composition of the environment:

- 316L in artificial seawater,

$$P_d = 26t^{0.6} \tag{9}$$

- and for 304 stainless steel, also in artificial seawater, the following equation:

$$P_d = 27.9t^{0.67} \tag{10}$$

where P_d is similar to *MPD* in μm and t is the polarization time in minutes.

The MPD generated on the 304 stainless steel in artificial sea water, reported by Gonzalez-Sanchez [40] were slightly lower, but with a trend similar to those obtained by Dzib-Pérez [55]. These forms contribute to assess the first stage of damage (pitting).

Newman [43] reported the pit growth under potentiostatic polarization on a 304 stainless steel in a 1M NaCl solution containing 0.04 M $Na_2S_2O_3$. The pits generated had a hemispherical morphology. These authors found good agreement between results obtained via Faraday's law and those obtained from microscopic analysis. Researchers had reported the pits growth under potentiostatic polarization on 304 and 316L stainless steels in artificial seawater (Gonzalez-Sanchez, 2002) and natural seawater [56]. The shape of pits generated at both stainless steels was semi-elliptical [40, 56]. Gonzalez-Sanchez [40] reported a good agreement between the results obtained from Scanning Reference Electrode Technique (SRET) measurements with those obtained of a method of material removal.

In the present document, pits were generated under potentiostatic polarization on 304 stainless steels in 3.5% wt NaCl solution and in natural seawater as well as at open circuit potential in a solution of 1M $FeCl_3$. The pits generated had hemispherical morphology as seen in Figure 10.

In order to determine the correct morphology (semi-elliptical or hemispherical) of pits generated in this investigation the volume of each pit was calculated according to the geometry of an ellipse or an sphere and compared with results obtained from the

chronoamperometries. The results indicate that the volumes calculated based on a spherical geometry are closer to the volume calculated from the chronoamperometry curves, as seen in Figure 11. Therefore, the volume of a pit, obtained from removal of material, calculated according to a spherical geometry was used for comparison and analysis with the results obtained using electrochemical techniques. The values of the volume per pit as a function of growth time were used to calculate the corresponding amount of dissolved material for a pit grown under potentiostatic control on 304 SS in 3.5 wt% NaCl solution and in seawater natural. In Figure 12 shows the amount of dissolved material, determined chronoamperometries and by a method of material removal, as a function of pits growth time on the 304 stainless steel in NaCl solution and in water natural sea. Also, the figure 13 illustrates the pit nucleation and growth process obtained from SRET Maps.

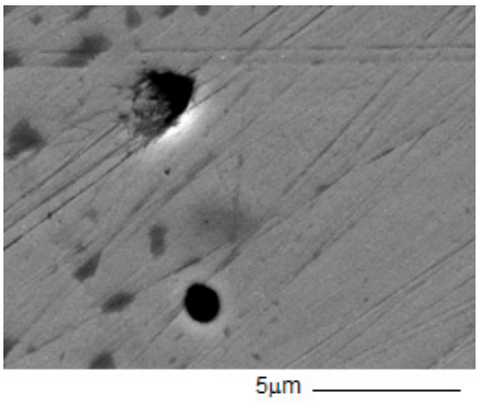

Figure 10. SEM image shows the pits potentiostatically generated in artificial seawater had hemispherical morphology on 316L steel surface under [40].

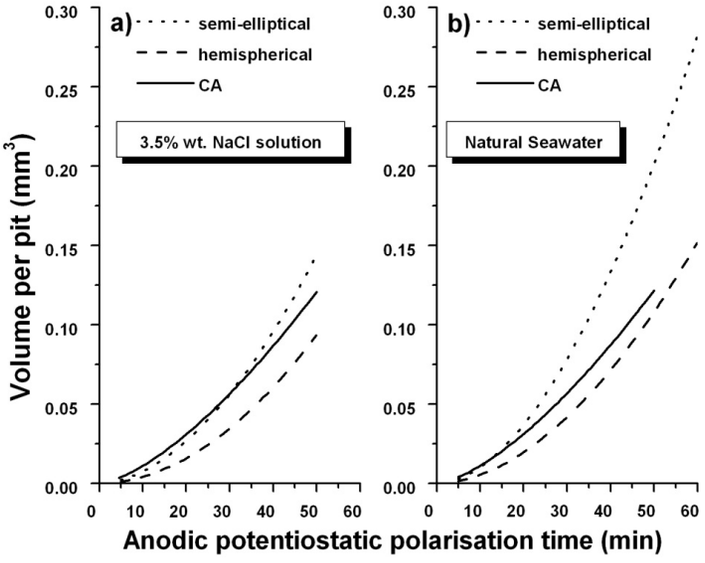

Figure 11. Comparison of the pits volume determined from the material removal method and from the integration of chronoamperometries for 304 SS in a) 3.5% NaCl and b) natural seawater [55].

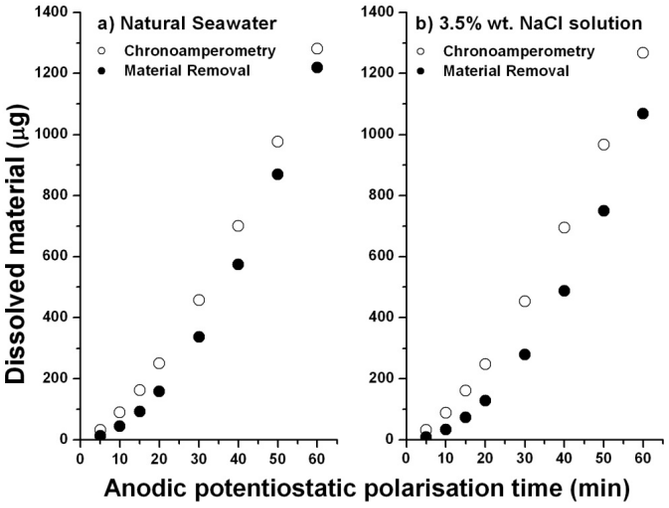

Figure 12. Amount of dissolved material per pit, determined from the chronoamperometries and by a method of material removal as a function of anodic polarization time for the 304 SS in a) natural seawater and b) 3.5% wt NaCl solution [55].

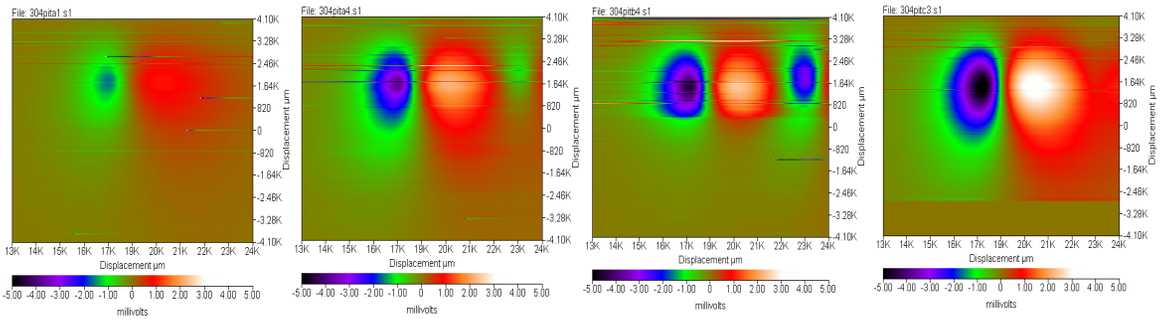

Figure 13. SRET map scans during pitting initiation and growth on 304 SS specimens polarized at 290 mV vs SCE for 2.3, 17.5, 37.5 and 56.5 minutes under fatigue loading conditions [40].

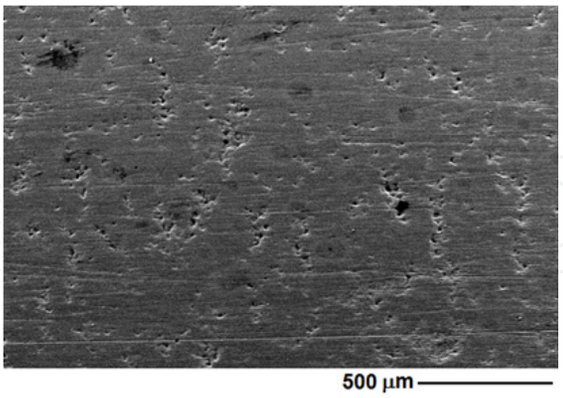

Figure 14. Pits formed at grain boundaries of a 316L SS undergoing cyclic loading in natural seawater. $\Delta\sigma$ = 140 MPa (58%σ0.2), after N=86400 cycles, at a load frequency ω=0.17 Hz, stress ratio R=0, T_{Ave}= 29°C and pH_{Ave} = 7.9. Patterns of grain boundaries are reveled practically in the image [56].

Acuña [56] has observed that on the maximum tensile stress zone of bent-beam specimens, after N loading cycles in natural seawater, the pits nucleation sites generally were located at grain boundaries on the specimen surface (Figure 14).

3.3. Pit to small crack transition

Pit to short crack transition involves the determination of the critical pit size for the transition from pit to fatigue crack. In this stage, the microstructure and the state of stresses around the corrosion pit play a very important role. The conditions for the pit to crack transition are generally defined phenomenologically by using a Linear Elastic Fracture Mechanics (LEFM) approach. A major concern is that the threshold stress intensity factor range defined for corrosion fatigue cracking is determined considering long cracks and can not be applied to microscopically small cracks (MSC) initiated from pits.

Two criteria are used to describe the transition processes:

- the stress intensity factor associated with the equivalent surface crack growth at which the corrosion pit reaches the threshold stress intensity factor for the fatigue crack growth,

$$(\Delta K)_{pit} = (\Delta K)_{crack}, \tag{11}$$

- Corrosion fatigue crack growth rate also exceeds the pit growth rate,

$$\left(\frac{da}{dt}\right)_{crack} \geq \left(\frac{da}{dt}\right)_{pit} \tag{12}$$

Akid et. al. [57] have shown that in some cases pit development overcomes the nucleation stage of the corrosion fatigue cracking process. However, it appears that transition from pit to short fatigue crack occurs at some critical size associated with microstructure, applied stress level, mode of load and stress state around the pit. In order to describe the stress state and the stress intensity conditions around the pit, several models, based in pitting corrosion fatigue mechanisms have been proposed [58-61]. They have been assumed that corrosion pits behave as sites for fatigue crack initiation through a purely mechanical micro-notch effect in smooth surfaces. Real components are normally undergoing complex stress conditions which induce mixed loading modes; where it has been reported that the threshold stress intensity factor for short fatigue cracks in structures subjected to mixed loading modes is lower than for structures subject to simple loading mode conditions [62].

The general aim of this section is dedicated to determine the influence of mixed stress conditions on the initiation of fatigue cracks from corrosion pits. Here we present the results obtained from the analysis of the stress state and the threshold stress intensity around hemispherical corrosion pits developed on austenitic stainless steel samples immersed in natural seawater. The concept of pits as surface semi-elliptic cracks is introduced throughout a linear elastic fracture mechanics analysis. Pit depth to major mouth axes ratio (a/c) and the effect of stress orientation were analyzed in terms of variations of the stress state and mixed load modes. Also the pit to short crack transition and short crack growth is reported through sensitive electrochemical techniques.

From the SEM analysis conducted on the metallic specimens after 15 days of immersion in natural seawater, semi-elliptic corrosion pits with different depth /major mouth axes (a/c

aspect ratio) values: 0.33, 0.47, 0.56, 0.62 and 0.74 were found. Figure 15 presents corrosion pits formed on the surface of a specimen after *N*= 130200 cycles of test in flowing natural seawater and the potential and current noise profiles.

Pits developed on grain boundaries, mainly at triple point grain boundary. Small cracks (~ 5 μm long) had grown from nucleation sites (Figure 15c). From the earliest stage, the cracks grew by interconnecting several smaller cracks following the grain boundary pattern. Crack nucleation events and the early crack growth could be associated with the patterns of quick drop and slow recovery, of amplitudes of 20 and 70 mV and current density between 0.10 and 0.60 μA/cm² where these signals had higher intensity and higher frequency. Small cracks could grow from a multitude of nucleation sites and coalesce to form large cracks in a relatively short time. Large intergranular crack growth events can be associated with those patterns of 200 mV in amplitude and a cathodic current density of 8.0 μA/cm² (in the figure 15 (a) indicated with ellipses on the potential and current EN patrons). The potential transients could be the result of crack wall dissolution and a possible long active dissolution out of the crack, associated to current transients related to cracking by the reduction processes, where the cathodic reaction consumes electrons that are removed from the surface and the electrochemical double layer present on metal surface, both external to the crack and on the crack walls.

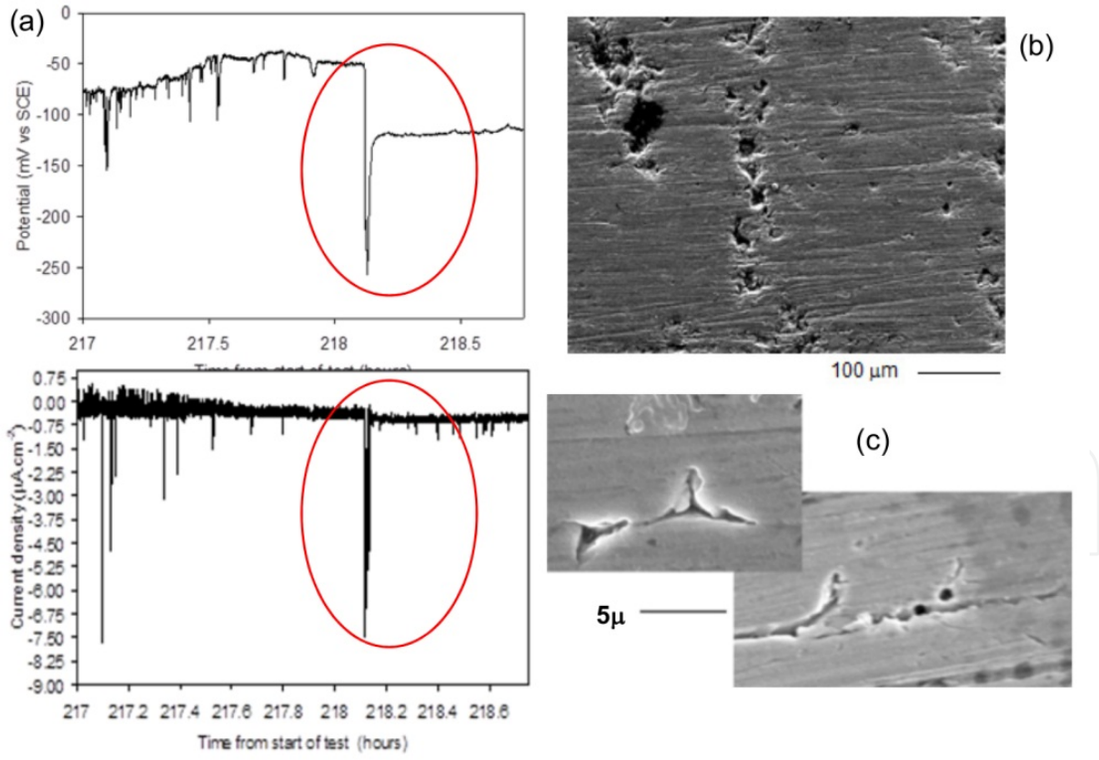

Figure 15. Corrosion pits developed on the stainless steel surface after *N*=130200 cycles of test in flowing natural seawater. $\Delta\sigma$= 140 MPa (58%$\sigma_{0.2}$), after *N*=130200 cycles, at a load frequency ω=0.17 Hz, stress ratio R=0, T_{Ave}= 29°C and pH_{Ave}= 7.9. (a) Potential and current noise (b) corrosion pits developed on grain boundaries [16] and (c) SEM photomicrograph showing CF small cracks formed at triple point and along grain boundaries.

In order understand the role of cyclic stress on pit development and growth, local electrochemical measurements were made using SRET on tubular samples of 316L steel immersed in 0.05% $FeCl_3$ solution pH~1.9, conductivity 11.6 mS/cm; under fatigue conditions with an applied stress range of 185 MPa (75%$\sigma_{0.2}$), ω=0.27 Hz, R=0. The crack appeared after ~700 load cycles. On figure 16 it can be seen that pit electrochemical activity increases with increasing number of applied cycles until the pit to crack transition occurs, which is associated with a drop in local pit current density [40].

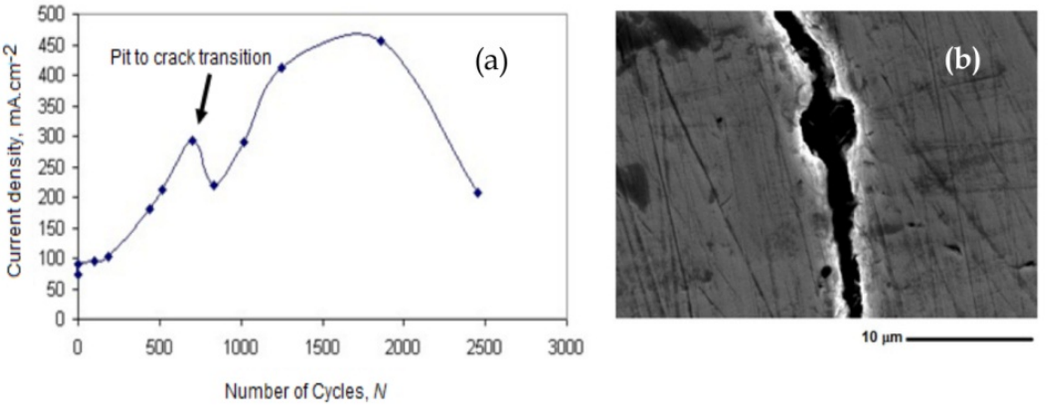

Figure 16. (a) Change in pit current density as function of number of fatigue cycles, indicated by the arrow, and (b) Crack growth from pit observed during corrosion fatigue test [40].

The current density at which the pit–crack transition occurs can then be used to determine the threshold stress intensity for the onset of cracking for damage from smooth surfaces. Figures 15(a) and 16(a) indicate that the first period was dominated by pitting corrosion and the CF cracks incubation took place; the second period corresponds to the nucleation and initial growth of short CF cracks from grain bonding triple points which is associated with a drastic decrease in potential (15 (a)) and current (16(a)). And finally, the third period where the electrochemical current noise signal recovered a synchronized pattern and also the current density from SRET measurements presented a change to higher values that may be related to the arrest of the CF cracks as their Faradaic contribution disappeared.

As above mentioned, the pit to a small crack transition is not governed solely by the stress distribution around the defect (pit), but is also determined by the local electrochemistry which controls pit growth, all together in a synergic phenomenon. We suggest that despite the solution chemistry is not be the same in large cracks as that found in inside a pit, and the microplasticity is generated by the stress concentration generated by the pit geometry for the case of austenitic stainless steels (susceptible to work hardening), the ΔK_{th} is a parameter that could be used to determine the stress intensity around of pit and pit contour. There are basically two reasons why the cyclic plastic deformation is higher just at the surface: concentration of plastic deformation due to higher stresses near the surface, and the low constraint on near-surface volumes of cyclically loaded material. In complex engineering components, higher surface stresses result from either micronotches (i.e. pits) or bending and twisting, both of which lead to stress gradients with the highest stress on the surface.

Usually, under conditions of uniaxial load, the geometry of a pit-like crack tends to keep a semicircular shape, whereas for the case of bending load, the surface cracks adopt a semi-elliptic configuration during their propagation [56]. It is for this reason that the direction of the applied stress plays an important role in the nucleation and propagation of fatigue cracks from corrosion pits.

In this section, the threshold stress intensity factor range (ΔK_{th}) was evaluated as a function of the aspect ratio (a/c) and the orientation of the corrosion pit with respect to the direction of the applied stress assuming tilted pits with hemispherical geometry, where in the case of fatigue limits based on crack propagation, corrosion pits act as cracks under conditions of linear elastic behavior [63-65]. The ΔK_I, ΔK_{II}, ΔK_{III} and ΔG were evaluated as a function of the applied stress direction (θ) assuming hemispherical pits, the position along the pit contour and also of the aspect ratio (a/c). Figure 17 presents the schematic of the stress element from which the transformed stresses as a function of the pit orientation angle are obtained.

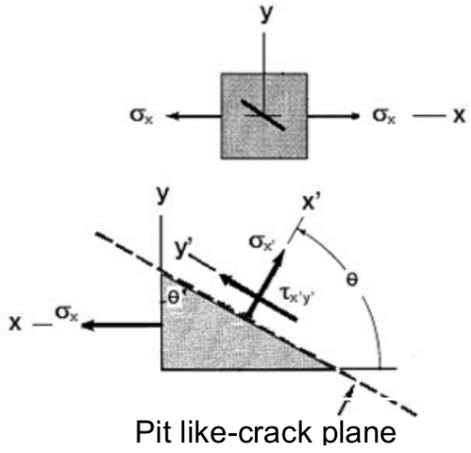

Figure 17. Stress state acting on a tilted hemispherical pit-like crack plane

Redefining the coordinate system to make the new axes coincide with the pit-like crack orientation, it is possible to resolve the applied stress on normal and tangential components. The relationship between the transformed stresses and the normal applied stress are given for equations (13) and (14).

$$\sigma_{x'} = \sigma_x \cos^2\theta \tag{13}$$

$$\tau_{x'y'} = \sigma_x \cos\theta \sin\theta \tag{14}$$

were $\sigma_{x'}$ and $\tau_{x'y'}$ are the normal and tangential stresses respectively as indicated in figure 18.

The stress components associated to the plane x'y' where the crack is located are $\sigma_{x'}$ y $\tau_{x'y'}$. The component $\sigma_{x'}$ induces load mode I whereas $\tau_{x'y}$ induces load mode II in the surface and load mode III at the bottom of the pit-like crack. Raju and Newman [66-67] proposed a solution for superficial hemispherical cracks; such a solution was based on finite element calculations.

$$\Delta K_I = \sigma_{x'} \sqrt{\frac{\pi a}{Q}} f(\phi) \tag{15}$$

$$f(\phi) = \left[\sin^2 \phi + \left(\frac{a}{c} \right)^2 \cos^2 \phi \right]^{\frac{1}{4}}$$

where a/c is ≤ 1, and φ specifies a particular position the stress level at around the tip of a hemispherical crack. Q is the shape factor of the defect or pit. The maximum value of ΔK_I occurs for $\varphi = 0°$, where $f(\varphi) = \sqrt{a/c}$, this is, near the surface over the major axis of the ellipse.

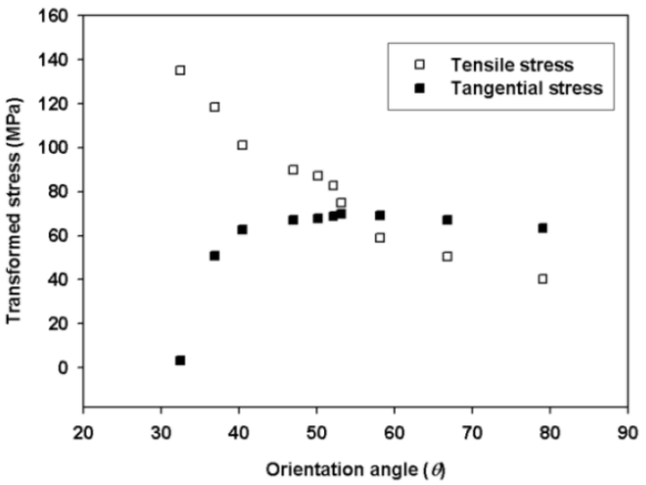

Figure 18. Relationship between the transformed stress acting around a pit-like crack and the orientation angle

The value of the threshold stress intensity factor for load mode II (ΔK_{II}) and III (ΔK_{III}) were calculated using the solution proposed for long elliptical surface cracks under mixed load mode [68]:

$$\Delta K_{II(\phi=0)} = \frac{\tau_{x'y'} \sqrt{\pi a} k^2 \left(a/c \right)^{1/2}}{B} \tag{16}$$

$$\Delta K_{III(\phi>0)} = \frac{\tau_{x'y'} \sqrt{\pi a} k^2 \left(1 - \nu \right) \sin \phi}{B \left[\sin^2 \phi + (a/c)^2 \cos^2 \phi \right]^{1/4}} \tag{17}$$

where k^2 = 1-(a/c)^2, B =(k^2 -ν)$E(k)$+ν(a/c)2$K(k)$ and $E(k)$ is the second order elliptic integral defined by:

$$E(k) = \sqrt{Q} = \int_0^{\pi/2} \sqrt{1 - k^2 \sin^2 \phi} d\phi \ , \ K(k) = \int_0^{\pi/2} \frac{d\varphi}{\sqrt{1 - k^2 \sin^2 \varphi}}$$

Equations 15, 16 and 17 were used to determine the stress intensity factor for load mode I, II and III respectively developed at the pit contour defined by the angle ϕ: (ϕ = 0°, ϕ = 45° and

$\phi = 90^{\circ}$). Considering two different normal applied stress values $\Delta\sigma_x = 217$ MPa ($90\%\sigma_{0.2}$) and $\Delta\sigma x$ = 140 MPa ($58\%\sigma_{0.2}$), with constant amplitude and a stress ratio R = 0. Normal and tangential stresses were simulated taking into account a system used by Acuña et al. [69], which allows changing sample orientation with respect to the applied stress direction for orientation angles $\theta > 0°$(Figure 17). Five different orientation angles (θ) were used: 0°, 30°, 45°, 60° and 75°. Figure 19 presents a schematic of the corrosion pit profile developed on the specimen surface using the electrochemical pit generation procedure.

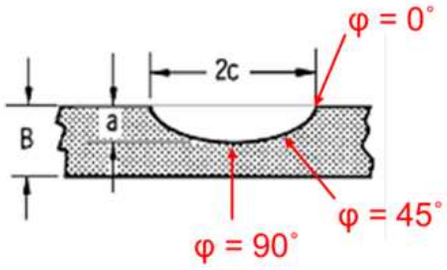

Figure 19. Schematic Corrosion pit contour developed on the stainless steel surface after electrochemical pre-pitting procedure in natural seawater.

Table 3, presents the values of ΔK_I, ΔK_{II} and ΔK_{III} as a function of the orientation angle θ, the aspect ratio a/c and the position around the pit profile ($\varphi = 0^{\circ}$, 45° and 90°).

In order to define the conditions for the initiation of fatigue cracks from pits on components subject to mixed load modes, a direct equivalence of stress intensity factor to the energy approach was considered. The approach where the elastic strain energy release rate (ΔG) related to the three load modes was considered.

$$\Delta G = \frac{(1-\nu^2)}{E}(\Delta K_I^2 + \Delta K_{II}^2) + \frac{(1-\nu)}{E}\Delta K_{III}^2 \tag{18}$$

Equation 18 indicates that ΔG depends upon the values of ΔK_I, ΔK_{II} and ΔK_{III} which are function of the orientation angle θ. It is worth mentioning that ΔK_{II} and ΔK_{III} do not have any contribution on ΔG for the case where θ is equal to zero.

Figure 20 shows the values of the ΔG as a function of the orientation angle for different locations along the pit contour: at the surface $\phi = 0^{\circ}$, at $\phi = 45^{\circ}$ and at the bottom of the pit where $\phi = 90^{\circ}$ for three different aspect ratio a/c values.

The fracture resistance value R in mode I, was also calculated and indicated in the graphics of figure 18. For the three considered a/c values, the maximum ΔG value was reached at θ = 45°in which the tangential stress predominates over the normal stress, independently of the position along the pit contour, which is more clearly showed in figure 21.

The orientation of the applied stress plays an important role in the nucleation and propagation of fatigue cracks from this kind of surface flaws (Figure 21). The asymmetry of the applied load induces normal and tangential stresses which along with the aspect ratio have a strong influence on the stress intensity factors which is observed in the variation of

ΔG vs orientation angle θ. Tangential stress has a coupled influence with tension stress for angles from 30° to 55° (load modes I, II and III).

Pit Contour		ϕ=0°			ϕ=90°		
		Maximum Stress Intensity Factor (MPa m$^{1/2}$)			Maximum Stress Intensity Factor (MPa m$^{1/2}$)		
Aspect ratio a/c	Mode Mixty (θ)	ΔK_I	ΔK_{II}	ΔK_{III}	ΔK_I	ΔK_{II}	ΔK_{III}
0.33	0°	100.87	0.00	0.00	176.94	0.00	0.00
	30°	75.66	36.91	52.99	132.71	36.91	52.99
	45°	50.44	42.62	61.19	88.47	42.62	61.19
	60°	25.22	36.91	52.99	44.24	36.91	52.99
	75°	6.76	21.31	30.59	11.85	21.31	30.59
	90°	0.00	0.00	0.00	0.00	0.00	0.00
0.47	0°	123.58	0.00	0.00	180.26	0.00	0.00
	30°	92.69	40.68	48.57	135.20	40.68	48.57
	45°	61.79	46.98	56.09	90.13	46.98	56.09
	60°	30.90	40.68	48.57	45.07	40.68	48.57
	75°	8.28	23.49	28.04	12.08	23.49	28.04
	90°	0.00	0.00	0.00	0.00	0.00	0.00
0.56	0°	134.36	0.00	0.00	179.55	0.00	0.00
	30°	100.77	41.42	45.30	134.66	41.42	45.30
	45°	67.18	47.83	52.31	89.77	47.83	52.31
	60°	33.59	41.42	45.30	44.89	41.42	45.30
	75°	9.00	23.91	26.16	12.03	23.91	26.16
	90°	0.00	0.00	0.00	0.00	0.00	0.00
0.62	0°	139.97	0.00	0.00	178.49	0.00	0.00
	30°	104.98	41.22	43.03	133.87	41.22	43.03
	45°	69.99	47.60	49.69	89.24	47.60	49.69
	60°	34.99	41.22	43.03	44.62	41.22	43.03
	75°	9.38	23.80	24.84	11.96	23.80	24.84
	90°	0.00	0.00	0.00	0.00	0.00	0.00
0.74	0°	150.23	0.00	0.00	175.24	0.00	0.00
	30°	112.68	38.65	36.90	131.43	38.65	36.90
	45°	75.12	44.62	42.61	87.62	44.62	42.61
	60°	37.56	38.65	36.90	43.81	38.65	36.90
	75°	10.06	22.31	21.30	11.74	22.31	21.30
	90°	0.00	0.00	0.00	0.00	0.00	0.00

Table 3. Stress Intensity Factor (MPa$\sqrt{m}$), ΔK_I, ΔK_{II} and ΔK_{III} as a function of θ, φ and a/c.

For angles lower than 30, tension stress are favoured (load mode I) and become the dominant stress. The orientation of the stress in an angle relative to the pit-like crack plane generates a normal tension stress at the microscopic plane of the crack that can be even higher than the externally applied stress. This induces a stress singularity that makes the perpendicular tension stress component sufficiently high to activate the crack initiation from the pit.

The analysis indicates that ΔG is higher in the surface where $\phi = 0^{\circ}$ (pit mouth) than at $\phi = 45^{\circ}$ and than at $\phi = 90^{\circ}$, (at the middle and at the bottom of the pit respectively) for inclination angles from 20° to 65° for a/c = 0.30. For the case of a/c = 0.60 and a/c = 0.75, the highest values of ΔG were observed at orientation angles from 5° to 75°. This result would indicate that the transition from pit to small crack takes place predominantly at the surface ($\phi = 0^{\circ}$), when the aspect ratio a/c→1 and the orientation angle θ increases, compared with those for ($\phi = 45^{\circ}$ and $\phi = 90^{\circ}$).

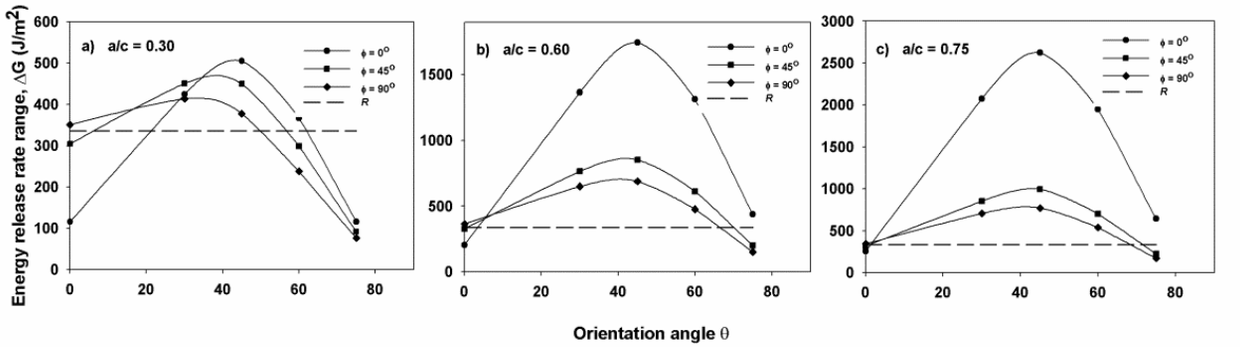

Figure 20. Energy release rate on semi-elliptic pits as a function of the orientation angle for three different values of a/c.: a) 0.30, b) 0.60 and c) 0.75.

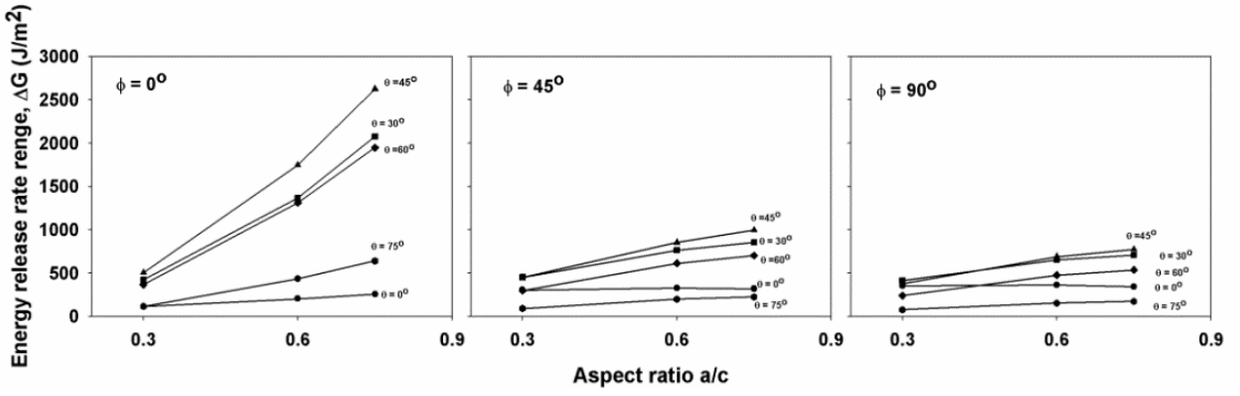

Figure 21. Energy release rate as a function of the aspect ratio for the 5 orientation angles at three different sites along the pit contour ($\varphi = 0^{o}$, $\varphi = 45^{o}$ and $\varphi = 90^{o}$).

Stress and strain distributions are viewed perpendicular to loading axis. Equivalent Von-Mises Stress and (b) total deformation of a pit with pit depth P_d=168μm. The plane stress had been assumed in the present analysis and the stress distribution around of semi-elliptic pit-like crack was done by considering biaxial loading conditions. Figures 22 and 23 show the Finite Element Analysis performed using ANSYS 11.0 [70]. A 3-D version of a thin-

walled 350 μm tube specimen was modeled and pits were created half way along the length of the specimen. A refined mesh was developed in the region around the pit to enhance the accuracy of stress and strain predictions. The von Mises criterion model was used in the analysis to characterize the elastic-plastic behaviour of the material. The FE model was applied to a hemispherical shaped pit of 168 μm, 274 μm and 291 μm deep. The aspect ratio is found to generally increase with increasing pit depth. Table 4 reports the results of ΔK and ΔG obtained for 3 pits depth configuration. Pit shape was obtained by a method of material removal and after modelled using Finite Element Method.

Specimen under cyclic loading at a stress level around 90% $\sigma_{0.2}$ exhibited a number of developed surface pits of 168μm deep. High stress and strain is observed on the figure 22. In the figure 22 (a), for biaxial stress conditions, the maximum stress is observed ϕ~45° at pit contour, near to the wall of the pit mouth, whereas the higher plastic strain is observed at the bottom of pit than just near to wall pit surface.

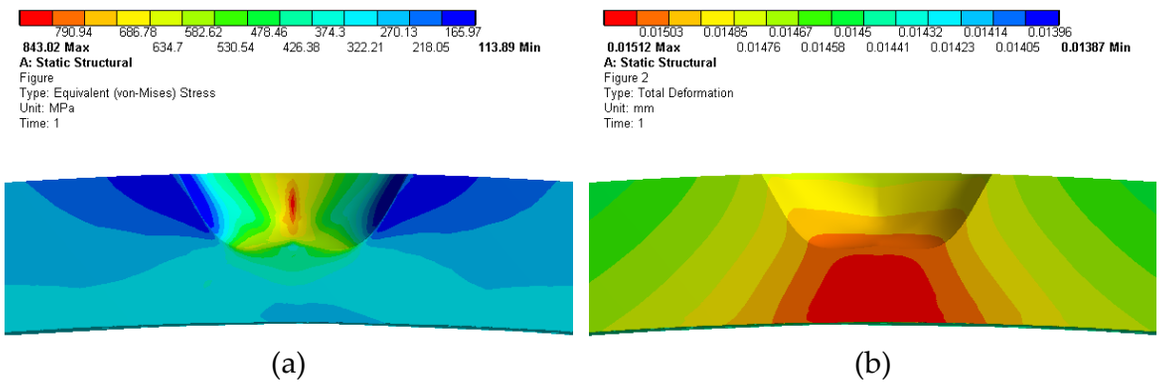

Figure 22. Maximum principal stress (a) and strain (b) distribution around a 168 μm hemispherical shaped pit developed on a pressured thin-walled 350 μm tube specimen made of 316L SS; $\sigma_{0.02}$= 241 MPa, *E*= 190 GPa and ν= 0.33. The internal pressure and the relation a/c were kept 110 bar and 0.67.

This plastic strain at pit bottom induces higher constrain than those observed just near to wall pit surface. Therefore, the pit to short crack transitions is done closer to the pit wall surface, as is shown in figure 22.

Location	Pit depth (μm)	Q	Hoop Stress (σ_1) (MPa)	Axial Stress (σ_2) (MPa)	Von-Mises Stress (MPa)	ΔG Hoop (J.m^{-2})	ΔG Axial (J.m^{-2})	ΔG Von-Mises (J.m^{-2})	ΔK_I Hoop (MPa m$^{1/2}$)	ΔK_I Axial (MPa m$^{1/2}$)	ΔK_I Von Mises (MPa m$^{1/2}$)
Pit: near to the surface	168	1.397	1100	407	831	1722.15	235.77	982.84	18.09	6.69	13.66
Pit bottom			433	10.1	388	266.85	0.146	214.27	7.12	0.16	6.38
Pit: near to the surface	274	1.466	502	157	478	531.21	51.96	481.65	10.04	3.14	9.56
Pit bottom			436	12.3	375	400.72	0.32	296.44	8.72	0.24	7.50
Pit: near to the surface	291	1.587	206	565	643	789.36	81.02	609.47	12.25	3.92	10.76
Pit bottom			33.7	388	396	299.47	2.168	287.37	7.54	0.64	7.39

Table 4. Results for FEM Analysis of 3 pit depth modeled in a pressured thin-walled 350 μm tube specimen made of 316L SS; $\sigma_{0.02}$= 241 MPa, E= 190 GPa and ν= 0.33. Q= Shape factor.

From figure 21 and table 3, it can be seen that for load mode I, when $\Delta K_{II}/\Delta K_I=0$, the value of ΔK_{Ith} is directly proportional to the aspect ratio. However, this relationship modifies as load mode II is dominant with respect to load mode I, ($\Delta K_{II}/\Delta K_I \sim 3$) at an angle of 75°, from which the values a/c = 0.47 and a/c = 0.74 seem to have no effect on ΔK_{eq}. It has been reported that for short fatigue cracks under conditions of mixed load mode, the value of the ΔK_{th} can be substantially smaller than that of long cracks [62]. Thus, it can be assumed that the condition for crack growth initiation is reached at ΔK_{eq} values lower than for single mode loading (ΔK_I, ΔK_{II} or ΔK_{III}).

Tangential stress has a coupled influence with tension stress for angles from 30° to 55° (load modes I and II). For angles lower than 30, tension stress are favoured (load mode I) and become the dominant stress.

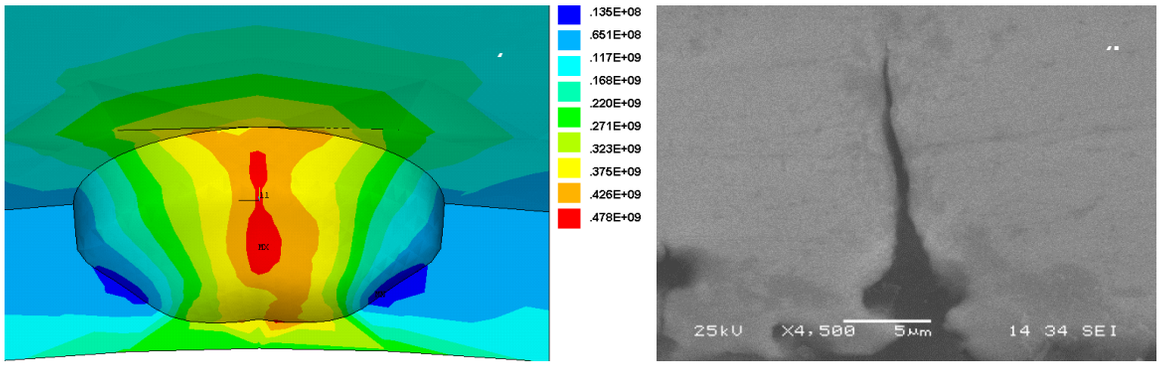

(a) (b)

Figure 23. (a) Maximum principal stress distribution at pit contour and (b) small crack emanating from a corrosion pit (Von-Mises: $\Delta K_{Isurface}$=9.56 MPa√m; $\Delta K_{Ibottom}$=7.50 MPa√m) , in a hemispherical shaped pit with a depth=291 µm and developed on a pressured thin-walled 350 µm tube specimen made of 316L SS; $\sigma_{0.02}$= 241 MPa, E= 190 GPa and ν= 0.33. The internal pressure and the relation a/c were kept 110 bar and 0.78.

The orientation of the stress in an angle relative to the pit-like crack plane generates a normal tension stress at the microscopic plane of the crack that can be even higher than the externally applied stress. This induces a stress singularity that makes the perpendicular tension stress component sufficiently high to activate the crack initiation from the pit. Based on the observations about the stress conditions around the pit-like cracks, the direction for crack initiation will be a function of the ratio, due to that the normal and tangential stresses vary with the orientation angle. Thus a crack will preferentially nucleate at sites of maximum principal normal stress as is indicated in figure 22 (a) and corroborated by figure 22 (b).

4. Conclusions

- From results obtained on corrosion fatigue tests using Electrochemical Noise and SRET, it was possible to determine the pit initiation time, pit activity and pit localization on specimen surface. The changes in dissolution current obtained from SRET

measurements and the increment in the amplitude and frequency of potential transients observed through the Electrochemical Noise tests, gave semi-quantitative information of the early stages of corrosion fatigue damage and cracking. Despite the inability to spatially resolve either the pit or crack size or shape from SRET measurements in $FeCl_3$, the change detected in electrochemical activity can be related to the transition from localized metal dissolution to crack nucleation; which may involve a redistribution of current over the new crack surfaces. Tests on corrosion fatigue, performed by the authors, were aimed to establish a relationship between Electrochemical Noise and SRET results in order to determine in a semi-quantitative base, the localized corrosion rate and the pit to crack transition process.

- FEM analysis corroborated that the local stress conditions for crack initiation in mixed mode, in a semi-elliptic surface pit, overcome the minimum stress level or single threshold stress established from the fatigue limit concept. Superposition of cyclic shear (ΔK_{II} or $\Delta K_{III} > 0$) to cyclic tension can lower the mode I threshold stress intensity range, ΔK_I, below which crack growth is presumed dominant.
- Based on ΔG data, crack initiation will mainly depend on the pit-like crack a/c ratio (α) as well as orientation angle (θ). From theoretical results, it could be assumed that the condition for crack growth initiation at the surface zone ($\phi = 0^\circ$) are favoured when $\alpha \geq 0.56$ and θ ranges from 5° to 75°, being the most manifest when $\theta \sim 45^\circ$.
- The alignment of corrosion pit with respect of the direction of applied nominal stress has a strong influence on the conditions for crack initiation. The crack initiation hot points are a function of a/c, θ and φ.

Author details

Narciso Acuña-González
Academic Vice-Chancellor Office, Anahuac-Mayab University, Merida, Mexico

Jorge A. González-Sánchez and Luis R. Dzib-Pérez
Centre for Corrosion Research, Autonomous University of Campeche, Campeche, Mexico

Aarón Rivas-Menchi
Faculty of Engineering, Anahuac-Mayab University, Merida, Mexico

5. References

[1] Miller K J (1987), Title. Fatigue Fract. Engng. Mater. Struct. 10 (1): p. 75.
[2] Sureh S (1998) Fatigue of Materials; second edition, Cambridge University Press. 679 p.
[3] Hagerup O, Strandmyr O (1998) Field experience with stainless steel materials in seawater systems. CORROSION-NACE 98, paper No. 707.
[4] Faimali M, Chelossi E, Pavanell G, Benedetti A, Vandecandelaere I, De Vos P, Vandamme P, Mollica A (2010) Electrochemical activity and bacterial diversity of natural marine biofilm in laboratory closed-systems. Bioelectrochem. 78: 30-38.

[5] Acuña N, Ortega-Morales B O, Valadez-Gonzalez A (2006) Biofilm colonization dynamics and its influence of austenitic UNS S31603 stainless steel exposed to Gulf of Mexico seawater. Mar. Biotechnol. 8: 62–70.
[6] Scotto V, Lai M E (1998) The ennoblement of stainless steels in seawater: a likely explanation coming from the field. Corros. Sci. 40:1007–1018.
[7] Mattila K, Carpen L, Raaska L, Alakomi H, Hakkarainen T, Salkinoja-Salonen MS (2000) Impact of biological factors on the ennoblement of stainless steel in Baltic seawater. J Indust Microbiol Biotechnol 24: 410–420
[8] Wang W, Wang J, Li X, Xu H, Wu J (2004) Influence of biofilm growth on corrosion potential of metals immersed in seawaters. Mater. Corros.. 55: 30–35.
[9] Gartland O P (1991) Aspects of testing stainless steels for seawater applications. Marine and Microbial Corrosion. p. 134
[10] Mansfeld F, Tsai R, Shih H, Little B, Ray R, Wagner P (1990) Results of exposure of stainless steels and titanium to natural seawater CORROSION NACE 90, paper No. 190
[11] Wei R P and Speidel M O (1972) Phenomenological aspects of corrosion fatigue, critical introduction. In: Corrosion Fatigue: Chemestry, Mechanics and Microstructure, NACE-2: 379-380.
[12] Jaske C E, Payer J H, Balint S V (1981) Corrosion Fatigue of Metals in Marine Environments. Springer – Verlag and Battelle Press. P.
[13] Kim K, Hartt W H (1995) Title. Journal of Offshore Mechanics and Artic Engineering, 117: p. 183.
[14] Akid R, Dmytrakh IM, Gonzalez-Sanchez J (2006) Fatigue Damage Accumulation: Aspects of Environmental Interaction. Materials Science, 42 (1): 42-53.
[15] Boukerrou and Cottis R.A.; (1993), Corrosion Science, 35, No. 1-4, p. 577.
[16] Acuña N (2005) Fatigue Corrosion Cracking of an Austenitic Stainless Steel Using Electrochemical Noise Technique. Anti. Corr. Meth. Mater. 52: 139-144.
[17] kid R., Dmytrakh I M, Gonzalez-Sanchez J (2006) Fatigue damage accumulation: the role of corrosion on the early stages of crack development. Corros. Engn. Science and Tech. 41 (4): 328-335
[18] Acuña-González N., García-Ochoa E., González-Sánchez J.; (2008), Assessment of the dynamics of corrosion fatigue crack initiation applying recurrence plots to the analysis of electrochemical noise data, Int. J. Fatigue 30:1211–1219.
[19] Horner D.A., Connolly B.J., Zhou S., Crocke L. and Turnbull A.; (2011) Novel images of the evolution of stress corrosion cracks from corrosion pits. Corrosion Science 53:3466–3485.
[20] Goswami T K, Hoeppner D W (1995) Pitting Corrosion Fatigue of Structural Materials. In: Chang C I, editor. Sun Structural Integrity in Aging aircraft. AD-Vol. 47. In: ASME, New York.
[21] Shreir L.L; (1976), "CORROSION Volume 1"second edition, Newnes-Butterworths, London U.K.
[22] Bockris J.O'M. and Reddy A.K.; (1970), "Modern Electrochemistry Vol. 2" Plenum Press, USA.

[23] Pourbaix M.; (1984), "On the Mechanisms, Teaching, and Research in Localised Corrosion", Journal of Electrochemical Society, Vol.131, No. 8
[24] Böhni, H.; (1987) " Localised corrosion in corrosion mechanisms", p. 285, Mansfeld and Dekker Eds
[25] Böhni H.; (1992), "Localised corrosion- Mechanisms and methods", Materials Science Forum Vols. 111-112, p. 401,Trans Tech Publications Switzerland.
[26] Williams D. E., Kilburn M. R., Cliff J., Waterhouse G.I.; (2010), "Composition changes around sulphide inclusions in stainless steels, and implications for the initiation of pitting corrosion", Corrosion Science 52:3702–3716
[27] Jones, D.; (1992), Principles and prevention of corrosion, Macmillan Publishing Co., N.Y., pg. 4.
[28] Marcus P., Olefjord I.; (1988), A Round Robin on combined electrochemical and AES/ESCA characterization of the passive films on Fe–Cr and Fe–Cr–Mo alloys, Corros. Sci. 28, 589–602.
[29] Mughrabi H., Wang R., Different K., and Essmann U., (1983); STP 811, American Society for Testing and Materials: p. 5
[30] Dawson, J.L., (1996), "ECN Measurement: The Definitive In-Situ Technique for Corrosion
[31] Legat, A. (1993), "EC Noise As the Basis of Corrosion Monitoring", Proceedings 12th International Corrosion Congress, NACE, Houston. 1410-1419.
[32] Dawson, J.L. et. al., (1989), "Corrosion Monitoring using ECN Measurements", Proceedings International Corrosion Congress, NACE, Houston, TX, Paper 89.
[33] Legat, A., Dolecek, V. (1995), "Corrosion Monitoring System Based on Measurement & Analysis of EC Noise", Corrosion Science, vol. 51 no. 4, pp. 295-307.
[34] Szklarska-Smialowska, Z; (1986), "Pitting Corrosion of Metals", NACE International, Houston, TX
[35] Benish, M.L., et.al. (1998), "A new electrochemical noise technique for monitoring the localized corrosion of 304 stainless steel in chloride-containing solutions", Proceedings International Corrosion Congress, NACE, San Diego, Paper 370
[36] Roberge, P.R., Wang, S. and Roberge, R. (1996); "Stainless steel pitting in thiosulfate solutions with Electrochemical Noise", Corrosion, vol. 52 no. 10, pp. 733-737
[37] Watanabe, Y. et.al., (1998), "Electrochemical noise characteristics of IGSCC in stainless steels in pressurized high-temperature water", Proceedings International Corrosion Congress, NACE, San Diego, Paper 129.
[38] Luo J., and Qiao L. J; (1999), "Application and evaluation of processing methods of electrochemical noise generated during Stress Corrosion Cracking", Corrosion, vol. 55 no. 9, pp. 870-876.
[39] González- Rodríguez, J. G., Salinas Bravo, V. M., García- Ochoa E. and Díaz Sánchez, A. (1997), "Use of electrochemical potential noise to detect initiation and propagation of stress corrosion cracking in a 17-4 PH steel", Corrosion, vol. 53 no. 9, pp. 693-699.
[40] González-Sánchez J. (2002); PhD thesis, Corrosion fatigue initiation in stainless steels: the scanning reference electrode technique, Sheffield Hallam University, Sheffield, UK.
[41] Djoudjou R., Lemaitre C., Beranger G.; (1993), Corrosion Reviews, Vol. 11, p. 157.

[42] Frankel G.S.; (1998) Pitting corrosion of metals – a review of the critical factors, Journal of the Electrochemical Society 145, 2186–2198
[43] Newman R.C., (2001);. Whitney W.R award lecture: understanding the corrosion of stainless steel, Corrosion 57, 1030–1041
[44] Sedriks A.J.; (1989), Corrosion - NACE, Vol. 45, p. 510.
[45] Sedriks A.J.; (1996), "Corrosion of Stainless Steels", second edition, John Wiley & Sons, Inc., USA
[46] Macdonald D.D.; (1992), J. Electrochem. Soc., Vol. 139, p.3434.
[47] Isaacs H.S. and Vyas B.; (1981), "Scanning Reference Electrode Techniques in Localised Corrosion", Electrochemical Corrosion testing, ASTM STP 727, p. 3, F.
[48] Bates S.J., Gosden S.R. and Sargeant D.A.; (1989), "Design and development of Scanning Reference Electrode Technique for investigation of pitting corrosion in FV 448 turbine disc steel", Materials Science and Technology, Vol. 5, p. 356
[49] Sargeant D.A., Hainse J.G.C. and Bates S.; (1989), " Microcomputer controlled scanning reference electrode apparatus developed to study pitting corrosion of gas turbine disc materials ", Materials Science and Technology, Vol. 5, p. 487
[50] Trethewey K.R., Marsh D.J. and Sargeant D.A.; (1996), "Quantitative Measurements of Localised Corrosion Using SRET", CORROSION-NACE 94, Paper no. 317.
[51] K.R. Trethewey, D.A Sargeant, D.J. Marsh and S. Haines, (1994), "New Methods on Quantitative Analysis of Localised Corrosion using Scanning electrochemical Probes", in Modelling Aqueous Corrosion: From individual Pits to System management, p. 417, eds. K.R. Trethewey and P.R. Roberge, Kluwer Academic Press.
[52] H.N. McMurray, S.R. Magill, and B.D. Jeffs (1996), "Scanning Reference Electrode Technique as a tool for investigating localised corrosion phenomena in galvanised steels", Iron and Steelmaking, Vol. 23, No.2, p 183
[53] H.N. McMurray and D.A. Worsley (1997), "Scanning Electrochemical Techniques for the Study of Localised Metallic Corrosion", in Research in Chemical Kinetics, Vol. 4, p. 149, Compton & Hancock eds. Blackwell Science Ltd
[54] Rosenfeld I L, Danilov IS (1967) Electrochemical Aspects of Pitting Corrosion. Corrosion Science, 7:129.
[55] Dzib-Pérez L., (2009), Ph.D. thesis, National Autonomous University of Mexico, Mexico.
[56] Acuña-González N.; (2001), Ph.D. Thesis, The effect of Micro-organisms on the Corrosion Fatigue Performance of Stainless Steel in Natural Seawater. National University of Mexico, Mexico.
[57] Akid R., Wang Y.Z., and Fernando U. S.; (1993) The Influence of Loading Mode and Environment on Short Fatigue Crack Growth in a High Strength Steel. Corrosion – Deformation Interactions (ed. T. Magnin and J. M. Gras), Les Editions de Physique, pp. 659-670.
[58] Hoeppner D.W.; (1979) "Model for Prediction of Fatigue Lives Based Upon a Pitting Corrosion Fatigue Process", Fatigue Mechanisms, Proceedings of an ASTM-NBS-NSF Symposium, J.T. Fong, De., ASTM STP 675, American Society for Testing and Materials, 1979 pp. 841-870.

[59] Lindley T.C., Mclntyre P. and Trant P. J.; (1982) "Fatigue Crack Initiation at Corrosion Pits," Metals Technology, Vol. 9, pp. 135-142.
[60] Kawai S., and Kasai K.; (1985) "Considerations of Allowable Stress of Corrosion Fatigue (Focused on the Influence of Pitting), "Fatigue Fracture of Engineering Materials Structure, Vol. 8, No. 2, pp. 115-127.
[61] Kondo Y.; (1983) "Prediction of Fatigue Crack Initiation Life Based on Pit Growth, "Corrosion Sciencie, Vol. 45, No.1, 1985, pp. 7-11.S. R. Novak, ASTM STP 801, p. 26
[62] Nalla RK, Campell JP, Ritchie RO; (2002) Fatigue Fract Engng Mater Strcut, 25
[63] Wei R. P; (1997) "Corrosion Fatigue – science and engineering" Conference of Recent Advances in Corrosion Fatigue", UK.
[64] Toyama K, Konda N; (1989) on International Conference of Evaluation of Materials Performance in Service Environments. Japan.
[65] Konda Y, and. Wei R. (1989), on International Conference of Evaluation of Materials Performance in Service Environments. Japan.
[66] Raju IS, Newman JC Jr.; (1979) Engineering Fracture Mechanics; 11
[67] Newman JC Jr, Raju IS (1981) Eng Fracture Mech;15
[68] He M, Hutchinson JW. (2000), Eng. Fract. Mech. 65
[69] Acuña-González N, González-Sánchez J, Contreras E, Sauceda I (2009) Effect of Mixed Mode Loading Induced by Asymmetrical Stress upon Crack Initiation from Corrosion Pits. Advanced Materials Research. 65:39-46.
[70] ANSYS® Academic Research, Release 11.0, license number: 34216380, Flex ID: 18a905230e25. ANSYS, Inc.